Rapid increase in summer surface ozone over the North China Plain during 2013–2019: a side effect of particulate matters reduction control?

Xiaodan Ma[1], Jianping Huang [2,6], Tianliang Zhao[1], Cheng Liu[3], Kaihui Zhao[4], Jia Xing[5], Wei Xiao[6]

[1]Collaborative Innovation Center on Forecast and Evaluation of Meteorological Disasters, Key Laboratory for Aerosol-Cloud-Precipitation of China Meteorological Administration, Nanjing University of Information Science and Technology, Nanjing 210044, China;

[2]I.M. System Group, Environmental Modeling Center, NOAA National Centers for Environmental Prediction, College Park, MD, USA

[3]Jiangxi Province Key Laboratory of the Causes and Control of Atmospheric Pollution/School of Water Resources and Environmental Engineering, East China University of Technology, Nanchang 330013, China

[4]School of Environment and Energy, South China University of Technology, Guangzhou 510006, China

[5]State Key Joint Laboratory of Environmental Simulation and Pollution Control, School of Environment, Tsinghua University, Beijing 100084, China

[6]Yale-NUIST Center on Atmospheric Environment, Nanjing University of Information Science and Technology, Nanjing, 210044, China

Correspondence to: Jianping Huang (jianping.huang@noaa.gov)

Abstract. While the elevated ambient levels of particulate matters with aerodynamic diameter of 2.5 micrometers or less ($PM_{2.5}$) are alleviated largely with the implementation of effective emission control measures, an opposite trend with a rapid increase is seen in surface ozone (O_3) in the North China Plain (NCP) region over the past several years. It is critical to determine the real culprit causing such a large increase in surface O_3. In this study, seven-year surface observations and satellite retrieval data are analyzed to determine the long-term change in surface O_3 as well as driving factors. Results indicate that anthropogenic emission control strategies and changes in aerosol concentrations as well as aerosol optical properties such as single-scattering albedo (SSA) are the most important factors driving such a large increase in surface O_3. Numerical simulations with National Center for Atmospheric Research (NCAR) Master Mechanism (MM) model suggest that reduction of O_3 precursor emissions and aerosol radiative effect accounted for 45 % and 23 % of the total change in surface O_3 in summertime during 2013–2019, respectively. Planetary boundary layer (PBL) height with an increase of 0.21 km and surface air

temperature with an increase of 2.1 °C contributed 18 % and 12 % to the total change in surface O_3, respectively. The combined effect of these factor was responsible for the rest change. Decrease in SSA or strengthened absorption property of aerosols may offset the impact of AOD reduction on surface O_3

35   substantially. While the MM model enables quantification of individual factor's percentage contributions, it requires further refinement with aerosol chemistry included in the future investigation. The study indicates an important role of aerosol radiative effect in development of more effective emission control strategies on reduction of ambient levels of O_3 as well as alleviation of national air quality standard exceedance events.

40   **1 Introduction**

Elevated ambient levels of ozone (O_3) are of great concern due to their important impact on human health, ecosystem productivity, atmospheric chemistry, and climate change (Monks et al., 2015; Tai et al., 2014; Tan et al., 2019). O_3 is produced by a series of photochemical reactions involving nitrogen oxides (NO_x = NO + NO_2) and volatile organic compounds (VOCs) in the presence of solar radiation. Ambient levels

45   of O_3 are highly dependent on emissions of O_3 precursors, solar radiation, and other physical processes such as regional and vertical transport (Sun et al., 2018; Ni et al., 2018; Liu et al., 2019; Wang et al., 2016b). While O_3 concentrations show a steady decreasing trend in Europe and North America, an opposite trend with an accelerating increase rate is observed in China (Lu et al., 2018; Li et al., 2019a). Due to high nonlinearity of O_3-NO_x-VOCs relationship and complexity of processes governing ambient

50   levels of O_3, a large uncertainty remains in the determination of impact of different driving factors on changes in surface O_3 concentrations under the polluted atmospheric conditions. Thus, accurate quantification of relative contributions of individual factors to the large increase in surface O_3 concentrations over the heavily polluted regions such as China continues to represent one of major challenges to research communities and government policy makers.

55   Anthropogenic emissions are the key in driving change in surface O_3. With rapid development of industrialization and urbanization, anthropogenic emissions of NO_x and VOCs, two major precursors of O_3 formation have been increasing significantly in China over the past several decades (Zeng et al.,2019). For instance, tropospheric columns of NO_2 ($TCNO_2$), an indicator of anthropogenic emission intensity of NO_x were increased by 307 % in Beijing from 1996 to 2011 (Huang et al., 2013), which caused a strong

60   increase trend of O_3 in the lower troposphere. Meanwhile, an increase in surface O_3 at a rate of 2 % a^{-1}

was observed in Beijing from 1995 to 2005 (Ding et al., 2007), and a similar increase with 1–2 ppb a^{-1}

was monitored at urban and remote sites in eastern China (Sun et al., 2016; Gao et al., 2017; Ma et al.,

2016; Tang et al., 2009). However, little light was shed on change in surface O_3 as compared to its

counterpart $PM_{2.5}$ which was elevated to the severe pollution level in eastern China especially over the

65   North China Plain (NCP) region (Zeng et al., 2019; Zhai et al., 2019). The severity of $PM_{2.5}$ pollution

has been largely alleviated after the stringent emission control strategies were implemented by Chinese

governments at national level in 2013 (Zeng et al., 2019). According to the estimate by Multi-resolution

Emission Inventory in China (MEIC), anthropogenic emissions of $PM_{2.5}$ decreased by approximately

60 %, NO_x emissions decreased by 21 %, significant reductions were also seen in other air pollutants

70   such as SO_2 but not for VOCs which showed an increase of 2 % instead over the period of 2013–2017

(Zheng et al., 2018). As a result, monthly mean $PM_{2.5}$ concentrations decreased by 41 % for the Beijing-

Tianjin-Hebei (BTH) region which is similar to the NCP region presented in this study, and aerosol

optical depth (AOD) was reduced by 20 % in eastern China (Li et al., 2019a). However, an opposite

trend with an accelerating increase rate of O_3 was observed in the NCP region during this period (Lu et

75   al., 2018; Cooper et al., 2014). The fact that O_3 formation was dominated by VOC-sensitive regime may

partly account for such an increase in the NCP region, but it is not clear how much the change of surface

O_3 is attributed to anthropogenic emission control efforts.

Aerosol radiative effect is another factor imposing a large constrain on change in surface O_3. Aerosols

attenuate surface-reached solar near-ultraviolet (UV) radiation effectively and reduce photolysis rate of

80   NO_2, a key parameter determining O_3 formation. Impact of aerosol radiative effect on photolysis rate of

NO_2 or O_3 photochemical production is highly dependent on aerosol optical properties as described by

AOD, single-scattering albedo (SSA), and asymmetry factor. AOD is a measure of extinction of solar

beam by aerosols (e.g., dust and haze), used as a proxy of representing severity of fine particulate-matter

pollution or aerosol mass concentrations. SSA denotes the relative contributions of scattering versus

85   absorption effect to total aerosol extinction efficiency with "0" for pure absorption and "1" for pure

scattering effect. Both numerical simulations and observations showed that aerosols with UV-scattering

effect may accelerate photochemical production of O_3 but aerosols with strong absorption property (e.g.

mineral dust and soot) may inhibit O_3 production in the atmospheric boundary layer (Dickerson et al.,

1997; Mok et al., 2016). The lowest photolysis rate coefficient was closely linked with the highest AOD

90   (Liu et al., 2019; Dickerson et al., 1997). It was observed that surface $PM_{2.5}$ concentrations decreased by

41 % whereas surface O_3 increased at a rate of 3.1 ppb a^{-1} over the BTH region from 2013 to 2017 (Li

et al., 2019a). Decrease in $PM_{2.5}$ was considered as one of the important causes leading to such an increase

in surface O_3 due to additional O_3 production associated with reduced sink of hydroperoxy radicals (HO_2)

(Li et al., 2019a). They pointed out that increase in surface O_3 associated with decrease in $PM_{2.5}$ was

95   more prominent than that with reduction of NO_x emissions over the NCP region where O_3 formation was

dominated by VOC-limited regime. Liu and Wang (2020a, 2020b) found the reduction of PM emissions

increased the O_3 levels by enhancing the photolysis rates and reducing heterogeneous uptake of reactive

gases (mainly HO_2 and O_3), of which the latter is more important than the former. Similar impact

associated with aerosol radiative properties on O_3 production was observed in other regions over the

100   world. For instance, the combined effect associated with optical properties of BrC and black carbon (BC)

reduced the net change in O_3 production by up to 18 % as compared to BC alone in the Amazon Basin

(Mok et al., 2016). Thus, surface O_3 changes are dependent on not only aerosol concentrations (AOD

used as a proxy) but also aerosol optical properties such as SSA. Relative importance of different aerosol

optical property parameters to change in surface O_3 needs to be addressed.

105   NCP, the largest alluvial plain of China, is surrounded by Mountains Yanshan with main peak of 2116

meters at the north, Mountains Taihang with the highest elevation of 2882 meters at the west, Mountains

Dabie and Tianmu at the south, and bordered to Yellow Sea at the east (see Fig. 1). Such a complex terrain

is not conducive to dispersion and dilution of air pollutants and makes them be trapped easily. Meanwhile,

the total energy consumption was increased by more than five times from 1985 to 2016 (Zeng et al.,

110   2019). NCP has become one of the most polluted regions in China. The highest $PM_{2.5}$ concentration

reached to $900 \mu g \cdot m^{-3}$ during winter and heavy $PM_{2.5}$ pollution events was the major concern to air

quality during that period (Gu, 2013; An et al., 2019), but surface $PM_{2.5}$ concentrations have reduced

substantially. Meanwhile, O_3 exceedance events became more frequent and more serious in the NCP

region (Zhang et al., 2015; Lang et al., 2017; Zhai et al., 2019). Hourly surface O_3 concentrations went

115   up to 150.0 ppb and the increase rate reached to 3.1 ppb a^{-1}, much higher than those observed in other

polluted regions such as Yangtze River Delta (YRD) and Pearl River Delta (PRD) in China (Li et al.,

2019a; Lyu et al., 2019). The elevated surface O_3 has become an emerging critical air quality issue in this

region (Wang et al., 2006; Shi et al., 2015). Understanding of the factors driving such as a rise in surface

O_3 becomes a very hot topic (Li et al., 2019a; Li et al., 2019b). However, most of the related studies are

120 limited to the contributions of atmospheric chemistry and changes in O_3 precursors' emissions. Relative importance of aerosol radiative effect associated with substantial decrease in aerosols or $PM_{2.5}$ and meteorological variability to the enhancement of surface O_3 is not well qualified.

In this study, seven-year air quality observational data provided by the China National Environmental Monitoring Center (CNEMC) Network are examined to determine the temporal and spatial variations in

125 surface O_3 over the NCP region over the period of 2013–2019. A series of analyses are presented to investigate the long-term change trend of surface O_3 and the statistical relationships with NO_x and VOCs emissions, meteorological variables, and aerosol radiative optical property parameters. A box model with Master Mechanism (MM) then is utilized to determine the response of surface O_3 to the key driving factors. The specific objectives include 1) to identify the key factors driving the increase in surface O_3

130 over NCP, the most polluted region in China; 2) to quantify the relative contributions of anthropogenic emissions (e.g., NO_x and VOCs), aerosol concentrations, aerosol optical properties, and meteorological variability to the increase in surface O_3 in summertime during 2013–2019.

2 Data and Methods

2.1 Observational data

135 Data used in this study include hourly-averaged surface observations of O_3 and $PM_{2.5}$ from 2013 to 2019 provided by the CNEMC (http://106.37.208.233:20035/). UV data measured at the Yucheng site (i.e., YCA, 116.57º E, 36.87º N) in the NCP region are obtained from the Chinese Ecosystem Research Network (http://www.cern.ac.cn/) from years 2013 to 2016. AOD is derived from the monthly level-3 product of the Moderate Resolution Imaging Spectroradiometer (MODIS) instrument aboard the Aqua

140 satellite, reported at 550-nm wavelength with resolutions of 1° × 1° (Platnick, 2015). $TCNO_2$ data are retrieved from the daily level-3 products of the Ozone Monitor Instrument (OMI) aboard the Aura satellite with resolutions of 0.25° × 0.25° (Nickolay A. Krotkov, 2019). Short-wave radiation data are provided by Land Data Assimilation System (FLDAS) (NASA, 2018) at resolutions of 0.1° × 0.1°. SSA retrieved from OMI/Aura Near UV Aerosol Optical Depth and Single Scattering Albedo V003

145 (OMAERUV) (Torres, 2006) at 388 nm are used to evaluate the impact of aerosol scatting/absorption properties on change in surface O_3. Daily max temperature at 2 m (T_{2max}), 10 m wind speed and the planetary boundary layer height (PBLH) are derived from the Modern-Era Retrospective Analysis for

Research and Applications version 2 (MERRA-2) reanalysis data at horizontal resolutions of 0.5° × 0.625° (Global Modeling and Assimilation Office, 2015).

150 **2.2 Model description and configurations**

The MM model is utilized to quantify the relative contributions of anthropogenic emissions and aerosol optical and radiative properties to the change in surface O_3. The MM is a chemistry box model, originally developed and updated by the scientists at National Center for Atmospheric Research (NCAR). It includes a detailed and flexible gas phase chemical mechanism consisting of approximately 5000

155 reactions for simulating temporal variations in chemical species of interest. The hydrocarbon chemistry in the MM is treated explicitly with photo-oxidation of partly oxygenated organic species included. Alkanes, alkenes and aromatics are considered as initial hydrocarbon reagents in the gas-phase mechanism. The Gear-type solver is used in the MM model to handle so large numbers of chemical reactions and species and the integration time steps varied during the simulations (Madronich and Calvert,

160 1989). The TUV model is called by the MM model for update of chemical reaction rates every fifteen minutes. This model computes time-dependent chemical evolution of an air parcel initialized with a known composition, assuming no additional emissions, no dilution and no heterogeneous processes. The MM model has been widely used to investigate impact of different factors such as emissions, chemistry, and meteorological conditions on simulations of O_3 and other chemical species (Liu et al., 2019; Geng

165 et al., 2007).

Photolysis rate j(NO_2) is calculated by using the Tropospheric Ultraviolet and Visible (TUV) radiation model which is embedded into the NCAR MM (Madronich S., 1999). In the fully-coupled system, the TUV is called by the MM model for update of photolysis rates of NO_2 and other chemical species (e.g., H_2O_2, O_3, NO_3, N_2O_5) every 15 minutes dynamically. The TUV model is initialized with the monthly

170 means of AOD, SSA, and total columns of O_3 retrieved from satellite measurements as well as other meteorological parameters such as cloud fractions at the central point of NCP (36° N, 117.5° E) in June.

HO_2 radicals are important to O_3 formation. The role of HO_2 radicals can be determined by the following reactions.

$$HO_2 + NO \rightarrow NO_2 + OH, \qquad\qquad R1$$

$$NO_2 + hv \rightarrow NO + O(^3P), \qquad\qquad R2$$

$$O_2 + O(^3P) \rightarrow O_3, \hspace{3cm} R3$$
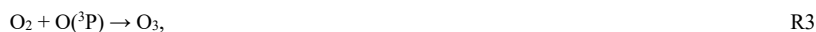
where hv represents ultraviolet radiation at the wavelengths of 200–400 nm. The MM model has a

175 capability of quantifying the role of radicals in O_3 formations under different pollution conditions.

The MM simulations are conducted for the predefined box as shown in Fig. 1 to represent ensemble mean behaviors and responses of the model to changes of different model inputs over the NCP region. The 24-hr simulations are conducted with the initial hour at 00z local time (LT). The inputs of the simulations include meteorological data (e.g., air temperature, cloud, and PBLH), aerosol radiative

180 properties (i.e., AOD and SSA), and emissions. While all the meteorological inputs are generated from observational data, the initial values of chemical species such as VOC species (e.g., Acrylic, 2-methylbutane, Toluene, P-xylene, Isoprene), N_2, O_2, H_2O, NO_2, O_3 etc. are obtained from climatology or background values.

Emissions (NO_x and VOCs) are calculated from the MEIC emission inventory. Aerosol radiative

185 property parameters from MODIS and OMAERUV are assumed as constants for all the simulations. All the simulations are driven by the monthly means averaged over the entire NCP region. The temporal variations at an interval of 4 hours are included in the model inputs to represent the diurnal variations in different meteorological variables such as T_{2max} and PBLH from MERRA-2 reanalysis.

Six groups with a total of sixteen numerical experiments with the MM model are designed to quantify

190 the roles of different factors in driving change in O_3 concentrations (Table 1). Case A stands for the base that the emissions were generated from MEIC in base year 2012 (http://www.meicmodel.org/) with an adjustment for year-2013 use, and the spatial distributions of NO_x and VOCs are presented in Fig. S1. Case B represents a scenario for year 2019 with NO_x and VOCs emission changes by -35% and $+10\%$ with respect to the case in year 2013, respectively. The changes in NO_x emissions (-35%) and VOCs

195 emissions ($+10\%$) in 2019 were obtained by extrapolating their respective changes during the period from 2013 to 2017 (Li et al., 2019a). Case C1 denotes a scenario with AOD decreased from 1.0 (i.e., the case for year 2013) to 0.75 (i.e., for year 2019) according to MODIS measurements and other six members in group C are used to examine the impact of varying AOD on the change in surface O_3. Case D1 is the one with a change of SSA from 0.95 (year 2013) to 0.93 (year 2019). Case E is a scenario with

200 T_{2max} increase from 29.9 ℃ in 2013 to 32.0 ℃ in 2019 based on regional average calculated with the MERRA-2 reanalysis in the NCP region. Case F is designed to assess the impact of the increased PBLH

(i.e., increase from 0.76 km in 2013 to 0.97 km in 2019) on surface O_3 change in the NCP region. Case G is for the situation mimic for year 2019 representing the combined effect of changes in emissions, AOD, SSA, T_{2max}, and PBLH. 24-hr simulations are completed for each case to quantify the contributions

205 of individual factors to the changes in surface O_3 from 2013 to 2019. More details of the numerical experiments are presented in Table 1.

3 Results and Discussion

3.1 Spatiotemporal variations in surface O_3, $PM_{2.5}$, AOD, and $TCNO_2$

Figure 2 shows a comparison of spatially distributed monthly means of the maximum daily 8-h average

210 (MDA8) O_3, 24-h average $PM_{2.5}$, AOD, and $TCNO_2$ over the eastern China in June between 2013 and 2019 derived from in-situ and satellite observations. It is clear that NCP was the most polluted region with the highest values of MDA8 O_3, $PM_{2.5}$, AOD, and $TCNO_2$ over the past decade. 24-h average $PM_{2.5}$ concentrations were higher than 75.0 $\mu g\,m^{-3}$ (the Grade II National Ambient Air Quality Standard, NAAQS defined for residential areas) at most of the monitoring stations across the NCP region in June

215 2013. The highest 24-h average $PM_{2.5}$ reached to 766.0 $\mu g\,m^{-3}$ and the corresponding AOD was 1.0. As compared to the well-established monitoring network of $PM_{2.5}$, observational sites for O_3 were pretty sparse except for the BTH, YRD, and PRD across the eastern China in 2013. While the $TCNO_2$ was 2 times higher than that observed in North America (Stavrakou et al., 2008), the exceedance events of the MDA8 O_3 were not frequently observed across eastern China in 2013. $PM_{2.5}$ was the major air pollutant

220 in the NCP region during that time period.

$PM_{2.5}$ concentrations, AOD, and $TCNO_2$ have been reduced substantially as a result of the implementation of strict anthropogenic emission reduction policy in 2013. For instance, monthly mean of $PM_{2.5}$ concentrations decreased from 95.5 $\mu g\,m^{-3}$ to 33.2 $\mu g\,m^{-3}$ with a percentage reduction of 65 %. Monthly mean AOD was reduced from 1.0 in 2013 to 0.75 in 2019, indicating that $PM_{2.5}$ continued

225 to decrease at a rate of $-10 \sim -11\,\%\,a^{-1}$ which was similar to that during 2013–2017 (Li et al., 2019a). On the other hand, a rapid increase in surface O_3 concentrations was observed in the NCP region over the past several years. The hot spots with the MDA8 O_3 higher than 75.0 ppb were extended to the entire NCP as well as the neighbor regions in 2019 (Fig. 2b). The highest MDA8 O_3 reached to 112.8 ppb in 2018, which was even higher than the level (110.0 ppb) observed in Los Angeles (Lin et al., 2017). As

230   compared to the cases observed in 2017 (Li et al., 2019a; Li et al., 2019b), air pollution events with

higher surface O_3 became more severe and more frequent. The frequency of NAAQS exceedance events

for surface MDA8 O_3 (i.e., greater than 160 $\mu g\,m^{-3}$) in June increased from 30 % in 2013 to 63 % in

2019. Here percentage represents the proportion of MDA8 exceedance days to a total of 30 days (i.e.,

June).

235   Reduction in NO_x emissions and slight increase in VOC emissions could be part of the reasons causing

such an increase over the NCP region where O_3 formation was dominated by VOC-limited regime.

Meanwhile, Li et al. (2019a) attributed the increase to aerosol chemistry that removal of HO_2 radicals

was reduced and more O_3 production was promoted. On the other hand, attenuation of UV radiation

became less evident as $PM_{2.5}$ or AOD continually decreased. Strengthening UV radiation may accelerate

240   photolysis of NO_2 and eventually led to more O_3 production. Importance of aerosol radiative effect in the

increase in surface O_3 via the way of accelerating photolysis of NO_2 can be further evaluated through

numerical experiments.

    Meteorological conditions are another critical factor affecting O_3 production. Typically, higher air

temperature is responsible for higher photochemical reaction rates and more O_3 photochemical

245   production (Porter and Heald, 2019). As shown in Fig. 3, NCP was the hottest spot region with T_{2max}

which was about 4.0 °C higher than that in the neighbor regions. In addition, increase rate of T_{2max} in the

NCP was larger than that observed in other regions in eastern China. T_{2max} and surface-reaching

shortwave radiation increased by 3 % and 7 %, respectively, over the past several years. In addition to

man-made factors such as urbanization and industrialization, decrease in aerosols (e.g., $PM_{2.5}$ and AOD)

250   could be an important factor driving such a rise in air temperature due to weakening aerosol radiative

effect.

3.2 Yearly changes in surface O_3 during 2013–2019 and driving factors

    As presented above, NCP was the most polluted region with extremely high ambient levels of air

pollutants. Surface O_3 showed a rapid increase over the period from 2013 to 2019 while $PM_{2.5}$ and other

255   pollutants such as NO_x experienced a significant reduction. O_3 has become a major air quality concern

in summer. June was the month with the highest monthly mean MDA8 O_3 concentrations (Fig. S2). In

this section, we attempt to investigate the yearly change rate and to identify the factors that drove such a

large increase in surface O_3 over the NCP region throughout the period of 2013-2019.

Figure 4 shows the yearly changes in monthly means of MDA8 O_3, $PM_{2.5}$, AOD, SSA, $TCNO_2$, T_{2max},

260 and PBLH over the NCP region in June from 2013 to 2019. The change in monthly mean of surface MDA8 O_3 showed an opposite trend to that of $PM_{2.5}$ concentrations and other air pollutants. The increase rate of monthly mean MDA8 O_3 (4.6 ppb a^{-1}) during 2013–2019 was much higher than that observed in the same region during the period of 2005–2015 (1.1 ppb a^{-1}) (Ma et al., 2016), and other regions such as Mountain Tai, YRD, Hong Kong, and North America where the changes were less than 2.1 ppb a^{-1}

265 during the similar time period (e.g., Sun et al., 2016; Gao et al., 2017; Wang et al., 2017; Xu et al., 2019). At the same time, a large decrease can be found from the time series of $PM_{2.5}$, AOD, and $TCNO_2$. It is noted that SSA also showed a decreasing trend (Fig. 4e). Decrease in SSA was likely due to the fact that reduction of inorganic aerosols (e.g., sulfate and nitrate) was larger than that of carbonaceous ones (Zhang et al., 2020). Another noticed feature is that MDA8 O_3 showed a decreasing trend in 2019 relative

270 to 2018, which was opposite to that during 2013–2018 (Fig. 4a). It is worth to witness the change trend in the coming years.

To understand the factors driving the change in surface O_3, a series of scatter plots are presented to examine the relationships between the surface MAD8 O_3 and individual factors such as aerosol optical properties (i.e., AOD and SSA), $TCNO_2$, T_{2max}, and surface-reaching short-wave radiation over the past

275 seven years in June (Fig. 5). The values discussed here represent the monthly means. MAD8 O_3 showed two different regimes with an opposite dependence of O_3 formation on $PM_{2.5}$ concentrations. The first regime showed a decrease trend with increasing surface $PM_{2.5}$ when $PM_{2.5}$ concentrations were less than approximately 140.0 $\mu g\,m^{-3}$ whereas the second one showed no trend with increasing $PM_{2.5}$ when $PM_{2.5}$ concentrations were higher than 140.0 $\mu g\,m^{-3}$. The first regime was highly related to aerosol

280 radiative effect, which has been discussed above. For the 2nd regime, the impact of aerosol radiative effect on surface O_3 photochemical production seemed very minor or even negligible. Instead, O_3 production was suppressed significantly and MAD8 O_3 concentrations were less than 20.0 ppb. In this case, removal of surface O_3 through titration of NO was not effective and surface O_3 showed an increase rather than a decrease trend with increasing NO_x concentrations under the strong NO_x conditions as indicated by

285 $TCNO_2$ higher than 40–45× 10^{15} (cm^{-2}) in the troposphere. Here the threshold value of 140.0 $\mu g\,m^{-3}$ represents an observed reality in this region but it needs to investigate whether such a threshold value exists in other regions.

Figures 5d–e further demonstrate the critical role of meteorological factors in change of surface O_3. MDA8 O_3 showed a near linear increasing trend with increasing T_{2max} and surface-reaching shortwave radiation with respective linear regression correlation coefficients of 0.88 and 0.93. Increase in T_{2max} and strengthening shortwave radiation caused by decrease in $PM_{2.5}$ (a proxy of aerosols) played a positive role in driving the increase in surface O_3 in the NCP region. On the other hand, MDA8 O_3 showed a decrease trend with 10 m wind speed (Fig. 5f). That may explain why improvement of stagnation atmospheric conditions may alleviate severity of surface O_3 pollution to some extents.

Enhancement of UV radiation resulting from reduction in surface $PM_{2.5}$ represents one of important mechanisms in driving increase in surface O_3 concentrations. It can be further illustrated by Fig. 6. While UV radiation displays a nonlinear decreasing trend with surface $PM_{2.5}$ concentrations, surface O_3 (hourly) shows a near linear increasing trend with surface-reached UV radiation. UV radiation attenuation approaches to a constant with a value of 0.1–0.3 MJ m^{-2} when surface $PM_{2.5}$ concentrations reach to around 300 $\mu g\ m^{-3}$ or above.

Analyses presented above demonstrate that all the exceedance events of MDA8 are observed under conditions with $PM_{2.5}$ less than 60 $\mu g\ m^{-3}$, $TCNO_2$ of equal to or less than 5.0×10^{15} (cm^{-2}), T_{2max} higher than 28.0 °C, and surface-reaching shortwave radiation stronger than 250.0 W m^{-2}. Reduction in aerosols (e.g., surface $PM_{2.5}$ as a proxy) concentrations may strengthen UV radiation, increase T_{2max}, and eventually promote more surface O_3 production.

3.3 Relative contributions of different driving factors to increase in surface O_3

In this section, the box model MM is utilized to quantify the relative contributions of individual driving factors to the increase in surface O_3 over the NCP region during 2013–2019. A simulation-observation comparison is presented to evaluate the performance of the MM model on simulations of surface O_3 (Fig. 7), of which the O_3 observations averaged over all the stations in NCP is considered as the standard observed concentrations. The simulated O_3 peak was about one hour later than the observation, which was likely due to uncertainty of emission inventory and other meteorological factors. Overall, the MM model was able to mimic the observed variation pattern and peak value as indicated by the correlation coefficient of 0.95 between simulated and observed O_3.

A series of numerical experiments were then completed with the MM model to quantify the relative

contributions of anthropogenic emissions (i.e., NO_x and VOCs), AOD, SSA, air temperature, and PBLH

to the change in surface O_3 over the NCP region during 2013–2019. The results are presented in Table 2.

The changes in emissions of O_3-precursors (i.e., NO_x and VOC_s) (i.e., Case B) and decrease of AOD (i.e.,

Case C1) were the two major contributors with their respective positive contributions of 45 % and 70 %

320 to the increment in surface O_3. But increase in surface O_3 associated with AOD reduction was largely

offset by the reduction in SSA. Moreover, air temperature played a non-negligible role and the increase

in T_{2max} accounted for 12 % of surface-O_3 enhancement (Case E). Meanwhile, the increase of PBLHs

also contributed about 18 % to the increment in surface O_3 (Case F). As indicated by Case G, the

combined effect by multiple factors was larger than the simple summation of individual factor's

325 contributions or the total percentage contributions by individual factor was less than 100 %. This is likely

due to the fact that O_3 production is not the linear function of individual factor's contribution. Complex

interplay among different factors may account for rest of the increase (i.e., 2 %).

It is not surprised that reduction in NO_x emissions brought about increase in surface O_3 since O_3

formation was dominated by VOC-limited regime in most parts of the NCP region. Several numerical

330 experiments were conducted to understand the mechanism of reduced $PM_{2.5}$ or AOD facilitating the

increase in surface O_3. It is known that photolysis rate of NO_2, $j(NO_2)$ plays a critical role in O_3 formation.

Parameter $j(NO_2)$ was highly dependent on aerosol optical properties such as AOD and SSA, as well as

solar zenith angle (θ) (Dickerson et al., 1997). As shown in Fig. 8a, decreasing AOD was conducive to

photolysis of NO_2 due to reduction of attenuated UV radiation entering the PBL. However, weakened

335 scattering or strengthened absorption property of aerosols (i.e., reduced SSA) may attenuate the UV

entering the PBL, deaccelerating photolysis of NO_2. Thus, decrease in SSA may counteract the impact

associated with decrease in AOD, which may slow down the increase in surface O_3 to some extents. In

addition, $j(NO_2)$ showed the highest value at noontime ($\theta = 0°$ or $\sec\theta = 1$) and tended to decrease

when θ became larger (i.e., early morning or late afternoon). Figure 8b further demonstrates that O_3

340 formation or MDA8 O_3 showed a near linear increasing trend with $j(NO_2)$. While decrease in $PM_{2.5}$

concentrations or AOD strengthened the UV amount entering the PBL reduction in SSA may counteract

impact of decreased AOD partially. But impact of AOD outpaced that of SSA. Thus, surface O_3 (e.g.,

MDA8 O_3) still showed a large increase with the combined effect of AOD and SSA over the past several

years.

345 Now let us turn our attention to O_3-chemistry in the varying polluted region. As illustrated in Fig. 9,

HO$_2$ radicals were sensitive to aerosol properties (i.e., AOD and SSA) but the sensitivity was highly relied on the solar zenith angle (θ). HO$_2$ radical was more sensitive to AOD or SSA in the afternoon than in the morning while photolysis rate of HO$_2$ is more sensitive to AOD or SSA. It is noted that higher net O$_3$ production is highly associated with the faster decrease in J(O$_3$) than J(NO$_2$) in the afternoon

350   (Gerasopoulos et al., 2006). HO$_2$ radical abundance reduced as aerosol optical property became more absorptive. This indicates that decrease in SSA may cause reduction of HO$_2$, less NO$_2$, and then less O$_3$ production. The HO$_2$ peak hour was matched well with that of O$_3$ peak (around 15 p.m. LT), further confirming its important role in O$_3$ formation. Decrease in AOD may accelerate production of HO$_2$ radicals or slow down their sink, which was conducive to production of NO$_2$ (Li et al., 2019a) but

355   decrease in SSA may offset its impact if aerosols show strong absorption property. Meanwhile, strengthened UV associated with weakened aerosol radiative effect was conducive to photolysis of NO$_2$. As a result, more O$_3$ is produced. This accounted for substantial increase in surface O$_3$ while PM$_{2.5}$ decreased over the past several years (2013 to 2019). The results are consistent with the finding by Li et al. (2019a).

360   **4 Discussions**

In this study, a box model NCAR MM with the detailed NO$_x$-VOC-O$_3$ chemistry included is utilized to quantify percentage contributions of emissions, aerosol optical properties, and meteorological variabilities to increase in surface O$_3$ over the NCP region during 2013–2019. The findings may provide more scientific evidence to policy makers on developing more effective control strategies on reduction

365   in ambient levels of O$_3$ as well as exceedance events. However, three points deserve further discussions.

First, the impact of aerosol radiative effect on surface O$_3$ formation is dependent on not only aerosol abundance (i.e., AOD) but also aerosol scattering/absorption property (i.e., SSA). Their impacts can be offset to some extents when AOD and SSA show the same change trend (either increase or decrease) or can be strengthened substantially when both AOD and SSA show an opposite change trend. Here the

370   study on the NCP region represents the first case since both AOD and SSA showed a decrease trend over the past several years. Even so, the combined impact of aerosol radiative effect due to reductions in AOD and SSA still contributed 23% of the total change in surface O$_3$ in the NCP over the past several years. This reminds us that the impact of aerosol radiative effect could be more substantial if both AOD and

SSA show an opposite change trend. Moreover, as compared to impact of change in AOD on surface O_3

375   formation (e.g., Dickerson et al., 1997; Wang et al., 2016a; Xing et al., 2015; Xing et al., 2017), studies

on impact of change in SSA on surface O_3 formation are fewer (Dickerson et al., 1997; Mok et al., 2016).

Thus, changes of individual aerosol radiative property parameters must be addressed carefully in order

to present more accurate quantification of impact of aerosol radiative effect on change in surface O_3.

Second, as presented above, the MM model as a box model with the detailed O_3-NO_x-VOCs

380   relationship allows us to quantify relative contributions of individual factors to increase in surface O_3.

Overall, the model results are comparable to those by using three-dimensional (3D) chemistry and

transport models (e.g., Liu and Wang 2020a, 2020b). The MM model indicates that reduction of

anthropogenic emissions of NO_x was the greatest contributor (45 %) to the increase in surface O_3 in the

NCP region during 2013–2019, which was larger than Li et al., (2019a) in summertime from 2013 to

385   2017 (about 10 %) but less than that of Sun et al. (2019) in July from 2003 to 2015 (63 %) over the

eastern China. Aerosol radiative effect was ranked as the 2nd contributor to the change in surface O_3 in

this region. The percentage contribution was found to be larger than that presented by other studies (Li

et al., 2019a; Xing et al., 2015). This is partly because this study is focused on the impact on MDA8 O_3

whereas their studies investigated the impact on diurnal variations of surface O_3. In addition, Li et al.,

390   (2019a and 2019b) and Liu and Wang (2020a and 2020b) pointed out that aerosol chemistry played the

most important role in the enhancement of surface O_3 in this region through modification of HO_2 radicals

that produce additional O_3 formation. However, the MM model does not include aqueous-phase

chemistry that has been implemented in the 3D meteorology/chemistry models (e.g., Li et al., 2019a; Liu

and Wang, 2020a, 2020b). Thus, inclusion of aerosol chemistry in a box model like MM is necessary to

395   provide more accurate assessment of impact of aerosol radiative effect on surface O_3 change.

Third, as compared to 3D meteorology/chemistry coupling model(s), box model does not include

complex physical processes such as regional transport, vertical diffusion, and cloud formation, etc.

Computational resource and workload that a box model requires are much less than that a 3D chemical

transport model needs. This may allow us to complete a series of designed numerical experiments to

400   quantify the roles of individual factors easily with limited computational resources. It is acceptable by

using a box model if terrains are relatively flat in the box, horizontal gradients of emissions and air

pollutant concentrations are not strong, and transport in and out reaches a relative equilibrium state. As

shown in Fig. S1 and Fig. 2, the NCP region defined in this study represents the most polluted part in

eastern China, anthropogenic emissions tend to distribute relatively uniform across the region. To this
405   extent, it is appropriate to examine O_3 formation and its response to changes of different factors such as
emissions, meteorological conditions, and aerosol radiative properties by using a box model in the NCP
region. It is reminded that some other factors such as background ozone are not included in our sensitivity
study due to their limited impact in this region, and the box model results present an ensemble-mean
behavior for the given box but need further evaluations by using a complex meteorology/chemistry
410   coupling model such as Weather Research and Forecasting model with Chemistry (WRF/Chem).

5 Summary and conclusions

In this study, seven-year long surface observational air quality data are presented together with satellite
retrieval measurements of $TCNO_2$, AOD and SSA to investigate long-term change trend of surface O_3
415   over the NCP region in summer from 2013 to 2019. A comprehensive statistical analysis is completed to
explore the relationship of MDA8 O_3 with $PM_{2.5}$ concentrations, tropospheric columns of NO_2, AOD,
and meteorological variables such as T_{2max}, surface-reaching shortwave radiation, wind speed, and PBLH.
A box model representing the O_3-NO_x-VOCs relationship is then utilized to quantify the relative
contributions of different driving factors to the increase in surface O_3 in the NCP region over the period
420   of 2013–2019.

The observational analysis indicates, while $PM_{2.5}$ concentrations continued to decrease with a rate of
9.5 $ug\ m^{-3}\ a^{-1}$, surface O_3 showed an accelerated increase trend at a rate of 4.6 ppb a^{-1} over the NCP
region during summertime from 2013 to 2019. Both decrease in $PM_{2.5}$ and reduction in $TCNO_2$ are the
two key factors leading to such an increase in surface O_3. The former is closely associated with the
425   attenuation of UV entering the PBL whereas the latter is related to the fact that O_3 photochemical
production in the NCP region is dominated by VOC-limited regime. The trend analysis of satellite
retrieval measurements revealed an obvious increase in T_{2max} at the rate of 0.34 °C a^{-1}, a rapid decrease
in AOD from 1.0 in 2013 to 0.75 in 2019, and a reduction in SSA from 0.95 to 0.93. The changes of both
T_{2max} and AOD were conducive to photochemical production of O_3 whereas the variability of aerosol
430   scattering/absorption property (i.e., decrease in SSA) may largely offset the impact of AOD reduction.

The sensitivity studies with the box model MM indicate that reduction of emissions (i.e., NO_x),

meteorological conditions, and aerosol radiative effect associated with decrease in aerosol concentrations were the three most important factors in driving such a large increase in surface O_3. They accounted for 45 %, 30 %, and 23 % of the total increase in surface O_3, respectively over the NCP region in summertime

435 during 2013-2019. For the meteorological contribution, increases in the PBLH and air temperature (e.g., T_{2max}) were responsible for 18 % and 12 % of the total change of surface O_3, respectively. The percentage contribution of aerosol radiative effect (23 %) represented the net changes caused by aerosol concentrations (i.e., AOD) and aerosol radiative property (scattering/absorption, SSA) (70 % vs. −47 %). The model results further demonstrated that decrease in SSA (i.e., more absorptive) may lead to reduction

440 in HO_2 radicals and NO_2 concentrations, and then less O_3 production, which may largely counteract impact of aerosol radiative effect associated with decrease in AOD.

  This study has a strong implication that development of more effective control strategies on surface O_3 reduction needs to consider impact of aerosol radiative effect as well as the change of aerosol scattering/absorption properties (i.e., AOD and SSA).

445 **Data availability:** Data used in this paper can be provided by Xiaodan Ma (xaiodanma_nuist@163.com) upon request.

Author contributions: JH came up with the original idea of this study. XM and JH designed the numerical simulations. XM conducted the data analysis and the first draft of manuscript and JH did the edit work. TZ, CL, KZ, JX and WX were involved in the scientific interpretation and discussions. All

450 the authors commented on the paper.

Competing interests: The authors declare that they have no conflict of interest.

Acknowledgments: This study was jointly funded by the National Natural Science Foundation of China (Grant no. 41575009, no. 91744209) and the National Key R & D Program Pilot Projects of China (2016YFC0203304).

455

References

An, Z., Huang, R., Zhang, R., Tie, X., Li, G., Cao, J., Zhou, W., Shi, Z., Han, Y., Gu, Z., and Ji, Y.: Severe haze in northern China: A synergy of anthropogenic emissions and atmospheric processes, National. Acad. Sciences., 116, 8657-8666, https://doi.org/10.1073/pnas.1900125116, 2019.

460 Cooper, O. R., Parrish, D. D., Ziemke, J., Balashov, N. V., and Zbinden, R. M.: Global distribution and trends of tropospheric ozone: An observation-based review, Elem. Sci. Anth., 2, 000029, http://doi.org/10.12952/journal.elementa.000029, 2014.

Dickerson, R. R., Kondragunta, S., ., Stenchikov, G., ., Civerolo, K. L., Doddridge, B. G., and Holben, B. N.: The impact of aerosols on solar ultraviolet radiation and photochemical smog, Science, 278,

465 827-830, https://doi.org/10.1126/science.278.5339.827, 1997.

Ding, A. J., Wang, T., Thouret, V., Cammas, J. P., and Nédélec, P.: Tropospheric ozone climatology over Beijing: Analysis of aircraft data from the MOZAIC program, Atmos. Chem. Phys., 8, 1-13, https://doi.org/10.5194/acp-8-1-2008, 2007.

Gao, W., Tie, X., Xu, J., Huang, R., Mao, X., Zhou, G., and Chang, L.: Long-term trend of O3 in a mega

470 City (Shanghai), China: Characteristics, causes, and interactions with precursors, Sci. Total. Environ., 603-604, 425-433, https://doi.org/10.1016/j.scitotenv.2017.06.099, 2017.

Geng, F., Zhao, C., Tang, X., Lu, G., and Tie, X.: Analysis of ozone and VOCs measured in Shanghai: A case study, Atmos. Environ., 41, 989-1001, https://doi.org/10.1016/j.atmosenv.2006.09.023, 2007.

Gerasopoulos, E., Kouvarakis, G., Vrekoussis, M., Donoussis, C., Mihalopoulos, N., and Kanakidou, M.:

475 Photochemical ozone production in the Eastern Mediterranean, Atmospheric Environment, 40, 3057-3069, https://doi.org/10.1016/j.atmosenv.2005.12.061, 2006.

MERRA-2 tavg1_2d_flx_Nx: 2d,1-Hourly,Time-Averaged,Single-Level,Assimilation,Surface Flux Diagnostics V5.12.4, Greenbelt, MD, USA, Goddard Earth Sciences Data and Information Services Center (GES DISC): https://doi.org/10.5067/7MCPBJ41Y0K6, access: 10 April 2020, 2015.

480 Half of Chinese live in haze: report: http://www.ecns.cn/cns-wire/2013/07-12/72889.shtml, access: 10 April 2020, 2013.

Huang, J., Zhou, C., Lee, X., Bao, Y., Zhao, X., Fung, J., RICHTER, Andreas, Liu, X., and Zheng, Y.: The effects of rapid urbanization on the levels in tropospheric nitrogen dioxide and ozone over East China, Atmos. Environ., 77, 558-567, https://doi.org/10.1016/j.atmosenv.2013.05.030, 2013.

485   Lang, J., Zhang, Y., Zhou, Y., Cheng, S., Chen, D., Guo, X., Chen, S., Li, X., Xing, X., and Wang, H.: Trends of PM2.5 and chemical composition in Beijing, 2000-2015, Aerosol. Air. Qual., 17, 412-425, https://doi.org/10.4209/aaqr.2016.07.0307, 2017.

Li, K., Jacob, D. J., Liao, H., Shen, L., and Bates, K. H.: Anthropogenic drivers of 2013-2017 trends in summer surface ozone in China, National. Acad. Sciences., 116, 422-427, https://doi.org/10.1073/pnas.1812168116, 2019a.

Li, K., Jacob, D. J., Liao, H., Zhu, J., Shah, V., Shen, L., Bates, K. H., Zhang, Q., and Zhai, S.: A two-pollutant strategy for improving ozone and particulate air quality in China, Nat. Geosci., 12, 906-910, https://doi.org/10.1038/s41561-019-0464-x, 2019b.

Li, P., Marco, A. D., Feng, Z., Anav, A., Zhou, D., and Paoletti, E.: Nationwide ground-level ozone measurements in China suggest serious risks to forests, Environ. Pollut., 237, 803-813, https://doi.org/10.1016/j.envpol.2017.11.002, 2018.

Lin, M., Horowitz, L. W., Payton, R., Fiore, A. M., and Tonnesen, G.: US surface ozone trends and extremes from 1980 to 2014: Quantifying the roles of rising Asian emissions, domestic controls, wildfires, and climate, Atmos. Chem. Phys., 17, 2943-2970, https://doi.org/10.5194/acp-17-2943-2017, 2017.

Liu, Q., Liua, T., Chen, Y., Xu, J., Gao, W., Zhang, H., and Yao, Y.: Effects of aerosols on the surface ozone generation via a study of the interaction of ozone and its precursors during the summer in Shanghai, China, Sci. Total. Environ., 675, 235-246, https://doi.org/10.1016/j.scitotenv.2019.04.121, 2019.

Liu, Y., Wang, T.: Worsening urban ozone pollution in China from 2013 to 2017 – Part 1: The complex and varying roles of meteorology, Atmos. Chem. Phys., 20, 6305-6321, https://doi.org/10.5194/acp-20-6305-2020, 2020a.

Liu, Y., Wang, T.: Worsening urban ozone pollution in China from 2013 to 2017 – Part 2: The effects of emission changes and implications for multi-pollutant control, Atmos. Chem. Phys., 20, 6323-6337, https://doi.org/10.5194/acp-20-6323-2020, 2020b.

Lu, X., Hong, J., Zhang, L., Cooper, O. R., and Zhang, Y.: Severe Surface Ozone Pollution in China: A Global Perspective, Environ. Sci. Tech. Let., 5, acs.estlett.8b00366-, 2018.

Lyu, X., Wang, N., Guo, H., Xue, L., Jiang, F., Zeren, Y., Cheng, H., Cai, Z., Han, L., and Zhou, Y.: Causes of a continuous summertime O3 pollution event in Jinan, a central city in the North China

515   Plain, Atmos. Chem. Phys., 19, 3025-3042, https://doi.org/10.5194/acp-19-3025-2019, 2019.

Ma, Z., Jing, X., Quan, W., Zhang, Z., Lin, W., and Xu, X.: Significant increase of surface ozone at a
rural site, north of eastern China, Atmos. Chem. Phys., 16, 3969-3977, https://doi.org/10.5194/acp-
16-3969-2016, 2016.

Madronich S, Calvert J. The NCAR Master Mechanism of the Gas Phase Chemistry - Version 2.0[J].

520   NCAR Technical Note, 1989.

Madronich, S., and Calvert, J. G.: Permutation reactions of organic peroxy radicals in the atmosphere, J.
Geophys. Res. Atmos., 95, 5697-5715, https://doi.org/10.1029/JD095iD05p05697, 1990.

Madronich S., F. S.: The Role of Solar Radiation in Atmospheric Chemistry, Handbook of Environmental
Chemistry, Springer, Berlin, Heidelberg, Boule, P. (Ed.), 1999.

525   Mok, J., Krotkov, N. A., Arola, A., Torres, O., Jethva, H., Andrade, M., Labow, G., Eck, T. F., Li, Z., and
Dickerson, R. R.: Impacts of brown carbon from biomass burning on surface UV and ozone
photochemistry in the Amazon Basin, Sci. Rep., 6, 36940, https://doi.org/10.1038/srep36940, 2016.

Monks, P. S., Archibald, A. T., Colette, A., Cooper, O., and Williams, M. L.: Tropospheric ozone and its
precursors from the urban to the global scale from air quality to short-lived climate forcer, Atmos.

530   Chem. Phys., 15, 8889-8973, https://doi.org/10.5194/acp-15-8889-2015, 2015.

FLDAS Noah Land Surface Model L4 Global Monthly 0.1 x 0.1 degree (MERRA-2 and CHIRPS),
Greenbelt, MD, USA, Goddard Earth Sciences Data and Information Services Center (GES DISC):
10.5067/5NHC22T9375G, access: 10 April 2020, 2018.

Ni, R., Lin, J., Yan, Y., and Lin, W.: Foreign and domestic contributions to springtime ozone over China,

535   Atmos. Chem. Phys., 18, 11447–11469, https://doi.org/10.5194/acp-18-11447-2018, 2018.

OMI/Aura NO2 Cloud-Screened Total and Tropospheric Column L3 Global Gridded 0.25 degree x 0.25
degree V3, NASA Goddard Space Flight Center, Goddard Earth Sciences Data and Information
Services Center (GES DISC): https://doi.org/10.5067/Aura/OMI/DATA3007, access: 10 April 2020,
2019.

540   MODIS Atmosphere L3 Monthly Product (08_L3). NASA MODIS Adaptive Processing System,
Goddard Space Flight Center http://dx.doi.org/10.5067/MODIS/MYD08_M3.006, access: 10 April
2020, 2015.

Porter, W. C., and Heald, C. L.: The mechanisms and meteorological drivers of the summertime ozone–
temperature relationship, Atmos. Chem. Phys., 19, 1680-7316, https://doi.org/10.5194/acp-19-

545   13367-2019, 2019.

Shi, C., Wang, S., Rui, L., Rui, Z., Li, D., Wang, W., Li, Z., Cheng, T., and Zhou, B.: A study of aerosol optical properties during ozone pollution episodes in 2013 over Shanghai, China, Atmos. Res. , 153, 235-249, https://doi.org/10.1016/j.atmosres.2014.09.002, 2015.

Stavrakou, T., Müller, J.-F., Boersma, K. F., De Smedt, I., and van der A, R. J.: Assessing the distribution
550   and growth rates of NOx emission sources by inverting a 10-year record of NO2 satellite columns, Geophys. Res. Lett., 35, L10801, https://doi.org/10.1029/2008GL033521, 2008.

Sun, L., Xue, L., Wang, T., Gao, J., Ding, A., Cooper, O. R., Lin, M., Xu, P., Wang, Z., Wang, X., Wen, L., Zhu, Y., Chen, T., Yang, L., Wang, Y., Chen, J., and Wang, W.: Significant increase of summertime ozone at Mount Tai in Central Eastern China, Atmos. Chem. Phys., 16, 10637–10650,
555   https://doi.org/10.5194/acp-16-10637-2016, 2016.

Sun, L., Xue, L., Wang, Y., Li, L., and Wang, W.: Impacts of meteorology and emissions on surface ozone increases over Central Eastern China between 2003 and 2015, Atmos. Chem. Phys., 19, 1455–1469, https://doi.org/10.5194/acp-19-1455-2019, 2019.

Tai, A. P. K., Martin, M. V., and Heald, C. L.: Threat to future global food security from climate change
560   and ozone air pollution, Nature. Clim. Change., 4, 817-821, https://doi.org/10.1038/nclimate2317, 2014.

Tan, Z., Lu, K., Jiang, M., Su, R., Wang, H., Lou, S., Fu, Q., Zhai, C., Tan, Q., Yue, D., Chen, D., Wang, Z., Xie, S., Zeng, L., and Zhang, Y.: Daytime atmospheric oxidation capacity in four Chinese megacities during the photochemically polluted season: A case study based on box model simulation,
565   Atmos. Chem. Phys. , 19, 3493-3513, https://doi.org/10.5194/acp-19-3493-2019, 2019.

Tang, G., Li, X., Wang, Y., and Xin, J.: Surface ozone trend details and interpretations in Beijing, 2001–2006, Atmos. Chem. Phys., 9, 8813-8823, https://doi.org/10.5194/acp-9-8813-2009, 2009.

OMI/Aura Near UV Aerosol Optical Depth and Single Scattering Albedo 1-orbit L2 Swath 13x24 km V003, Greenbelt, MD, USA, Goddard Earth Sciences Data and Information Services Center (GES
570   DISC): https://doi.org/10.5067/Aura/OMI/DATA2004, access: 10 April 2020, 2006.

Wang, J., Allen, D. J., Pickering, K. E., Li, Z., and He, H.: Impact of aerosol direct effect on East Asian air quality during the EAST-AIRE campaign, J. Geophys. Res. Atmos., 121, 6534-6554, https://doi.org/10.1002/2016JD025108, 2016a.

Wang, T., Ding, A., Gao, J., and Wu, W. S.: Strong ozone production in urban plumes from Beijing, China,

575   Geophys. Res. Lett., 33, L21806, https://doi.org/10.1029/2006GL027689, 2006.

Wang, T., Xue, L., Brimblecombe, P., Yun, F. L., Li, L., and Zhang, L.: Ozone pollution in China: A review of concentrations, meteorological influences, chemical precursors, and effects, Sci. Total. Environ., 575, 1582-1596, https://doi.org/10.1016/j.scitotenv.2016.10.081, 2016b.

Wang, Y., Wang, H., Guo, H., Lyu, X., Cheng, H., Ling, Z., Louie, P. K. K., Simpson, I. J., Meinardi, S.,
580   and Blake, D. R.: Long-term O3–precursor relationships in Hong Kong: field observation and model simulation, Atmos. Chem. Phys., 17, 10919-10935, https://doi.org/10.5194/acp-17-10919-2017, 2017.

Xing, J., Mathur, R., Pleim, J., Hogrefe, C., Gan, C. M., Wong, D. C., Wei, C., and Wang, J.: Air pollution and climate response to aerosol direct radiative effects: A modeling study of decadal trends across
585   the northern hemisphere, J. Geophys. Res. Atmos., 120, 12,221–212,236, https://doi.org/10.1002/2015JD023933, 2015.

Xing, J., Wang, J., Mathur, R., Wang, S., Sarwar, G., Pleim, J., Hogrefe, C., Zhang, Y., Jiang, J., Wong, D. C., and Hao, J.: Impacts of aerosol direct effects on tropospheric ozone through changes in atmospheric dynamics and photolysis rates, Atmos. Chem. Phys., 17, 9869-9883,
590   https://doi.org/10.5194/acp-17-9869-2017, 2017.

Xu, X., Zhang, T., and Su, Y.: Temporal variations and trend of ground-level ozone based on long-term measurements in Windsor, Canada, Atmos. Chem. Phys., 19, 7335-7345, https://doi.org/10.5194/acp-19-7335-2019, 2019.

Zeng, Y., Cao, Y., Qiao, X., Seyler, B. C., and Tang, Y.: Air pollution reduction in China: Recent success
595   but great challenge for the future, Sci. Total. Environ., 663, 329-337, https://doi.org/10.1016/j.scitotenv.2019.01.262, 2019.

Zhai, S., Jacob, D. J., Wang, X., Shen, L., Li, K., Zhang, Y., Gui, K., Zhao, T., and Liao, H.: Fine particulate matter (PM2.5) trends in China, 2013–2018: separating contributions from anthropogenic emissions and meteorology, Atmos. Chem. Phys., 19, 11031-11041,
600   https://doi.org/10.5194/acp-19-11031-2019, 2019.

Zhang, F., Wang, Y., Peng, J., Chen, L., Sun, Y., Duan, L., Ge, X., Li, Y., Zhao, J., Liu, C., Zhang, X., Zhang, G., Pan, Y., Wang, Y., Zhang, A. L., Ji, Y., Wang, G., Hu, M., Molina, M. J., and Zhang, R.: An unexpected catalyst dominates formation and radiative forcing of regional haze, Proceedings of the National Academy of Sciences, 117, 3960-3966, https://doi.org/10.1073/pnas.1919343117,

605   2020.

Zhang, Z., Zhang, X., Gong, D., Quan, W., Zhao, X., Ma, Z., and Kim, S. J.: Evolution of surface O 3
        and PM 2.5 concentrations and their relationships with meteorological conditions over the last
        decade in Beijing, Atmos. Environ., 108, 67-75, https://doi.org/10.1016/j.atmosenv.2015.02.071,
        2015.

610   Zheng, B., Tong, D., Li, M., Liu, F., Hong, C., Geng, G., Li, H., Li, X., Peng, L., Qi, J., Yan, L., Zhang,
        Y., Zhao, H., Zheng, Y., He, K., and Zhang, Q.: Trends in China's anthropogenic emissions since
        2010 as the consequence of clean air actions, Atmos. Chem. Phys., 18, 14095-14111,
        https://doi.org/10.5194/acp-18-14095-2018, 2018.

615

620

625

630

635

Table 1. A summary of numerical experiments with the NCAR MM model.

Case	NOx emission	VOCs emission	AOD	SSA	T_{2max} (°C)	PBLH (km)
A	2013[*]	2013[*]	1.0	0.95	29.9	0.76
B	**2019[+]**	**2019[+]**	1.0	0.95	29.9	0.76
C1	2013	2013	**0.75**	0.95	29.9	0.76
D1	2013	2013	1.0	**0.93**	29.9	0.76
E	2013	2013	1.0	0.95	**32.0**	0.76
F	2013	2013	1.0	0.95	29.9	**0.97**
G	**2019**	**2019**	**0.75**	**0.93**	**32.0**	**0.97**
C2	2013	2013	**0.5**	0.95	29.9	0.76
C3	2013	2013	**0.6**	0.95	29.9	0.76
C4	2013	2013	**0.7**	0.95	29.9	0.76
C5	2013	2013	**0.8**	0.95	29.9	0.76
C6	2013	2013	**0.9**	0.95	29.9	0.76
C7	2013	2013	**1.1**	0.95	29.9	0.76
C8	2013	2013	**1.2**	0.95	29.9	0.76
C9	2013	2013	**1.25**	0.95	29.9	0.76
D2	2013	2013	1.0	**0.94**	29.9	0.76

640   [*]Year 2013: NO_x emission is 2.0×10^{12} mole. cm^{-2} s^{-1}, and VOCs emission is 7.3×10^{9} mole. cm^{-2} s^{-1}

[+]Year 2019: NO_x emission is 1.3×10^{12} mole. cm^{-2} s^{-1}, and VOCs emission is 8.0×10^{9} mole. cm^{-2} s^{-1}.

645

Table 2. Relative percentage contributions of emissions (case B), AOD (case C1), SSA (case D1), air temperature (case E), and PBLH (case F) to the change in MDA8 O_3 over the NCP region during 2013–2019.

	MDA8 O_3 (ppb)	Concentration Change (ppb)	Percentage Change (%)	Percentage Contribution (%)
A	55.35			
B	59.25	3.90	+ 7 %	+ 45 %
C1	61.46	6.11	+ 11 %	+ 70 %
D1	51.22	− 4.13	− 7 %	− 47 %
E	56.43	1.08	+ 2 %	+ 12 %
F	56.95	1.60	+ 3 %	+ 18 %
G	64.09	8.74	+ 16 %	

650
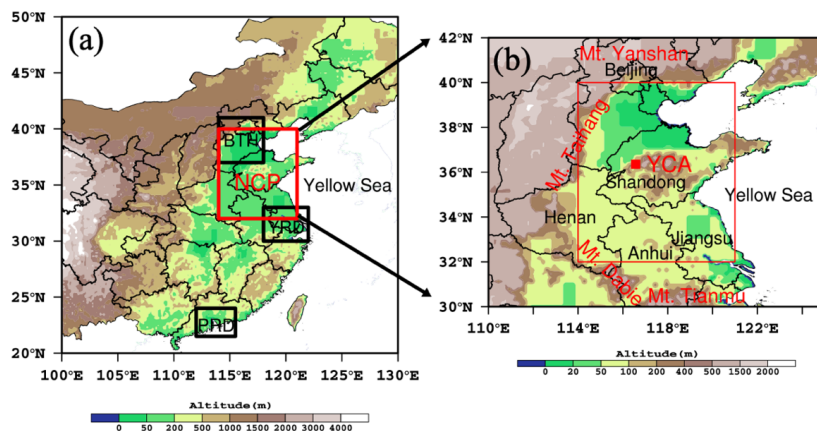
Figure 1. (a) Locations of North China Plain (NCP,32°–40° N, 114°–121° E) and other three major air pollution regions, Beijing-Tianjin-Hebei (BTH,37°–41° N, 114°–118° E), Yangtze River Delta (YRD, 30°–33° N, 118°–122° E), and Pearl River Delta (PRD, 21.5°–24° N, 112°–115.5° E) in China with terrain heights included and (b) location of ultraviolet (UV) radiation observational site, YCA (Yucheng site), areas covered by the NCP region and mountains surrounded.
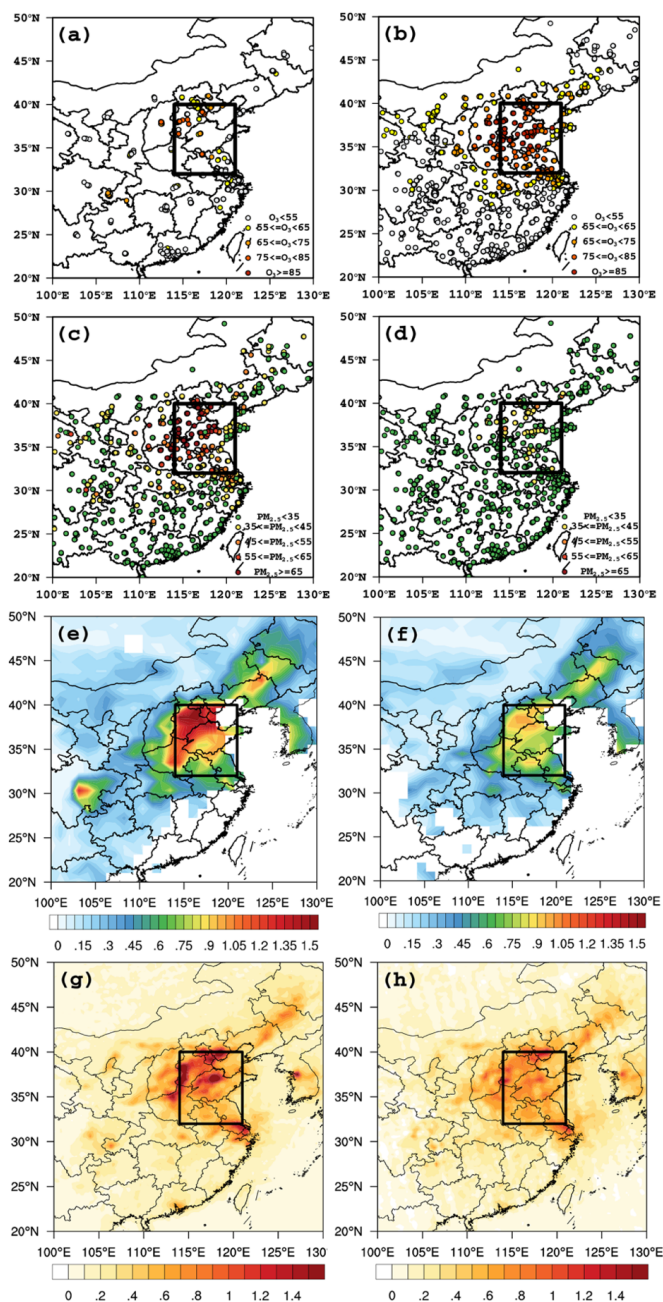
Figure 2. A comparison of spatial distributions of monthly mean of MDA8 O_3 (ppb) (a, b) and $PM_{2.5}$ (µg m^{-3}) (c,

d) obtained from in-situ observations, AOD (e, f) and tropospheric column of NO_2 ($TCNO_2$, 10^{16} cm^{-2}) (g, h) derived

from satellite observations between 2013 (in left column) and 2019 (in right column) in eastern China (NCP indicated

by the box).
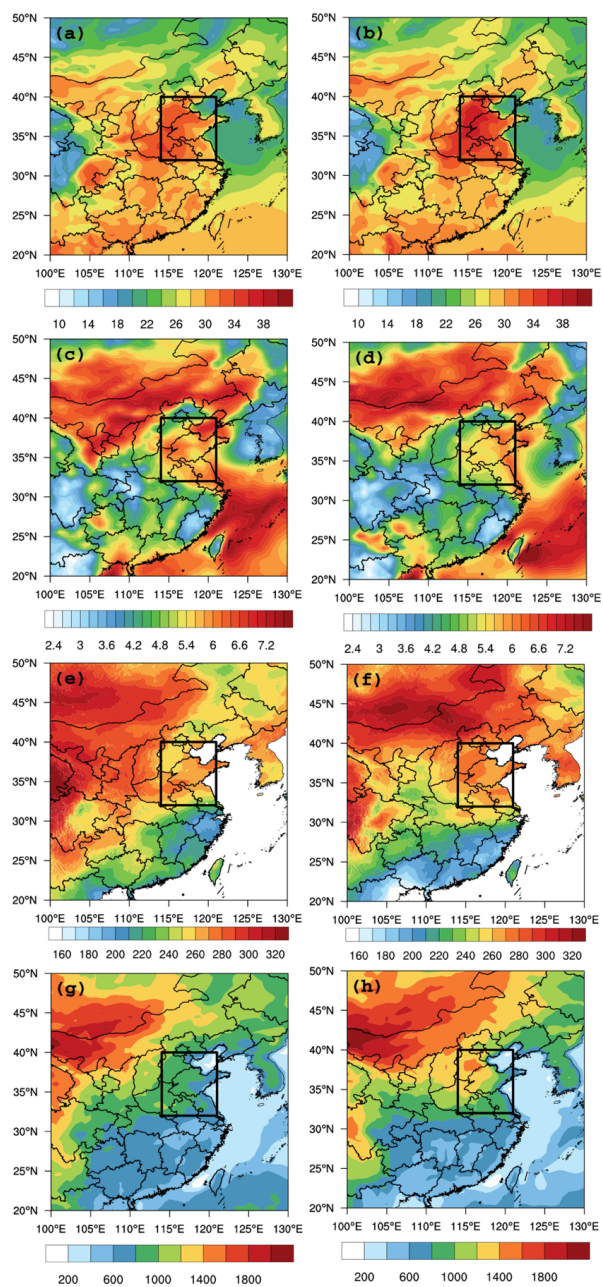
Figure 3. A comparison of spatial distributions of monthly mean of T_{2max} (°C, a and b), wind speed (m s^{-1}, c and d),

665   surface reaching short-wave radiation (W m^{-2}, e and f) and PBLH (m, g and h) between 2013 (in left column) and

2019 (in right column) in eastern China (the NCP indicated by the box).
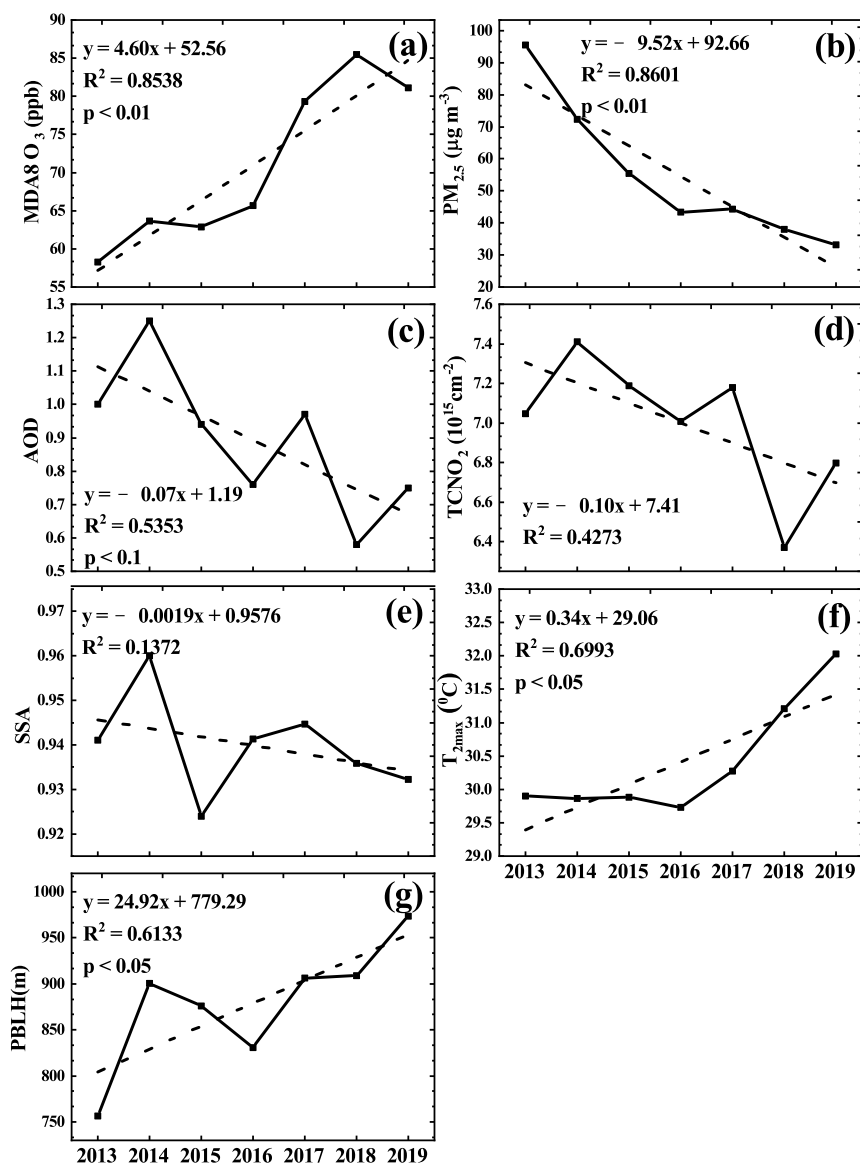
Figure 4. Long-term changes in monthly mean of (a) MDA8 O_3, (b) $PM_{2.5}$, (c) AOD, (d) $TCNO_2$, (e) SSA, (f)

670   T_{2max}, and (g) PBLH averaged over the North China Plain in June over the period of 2013–2019.
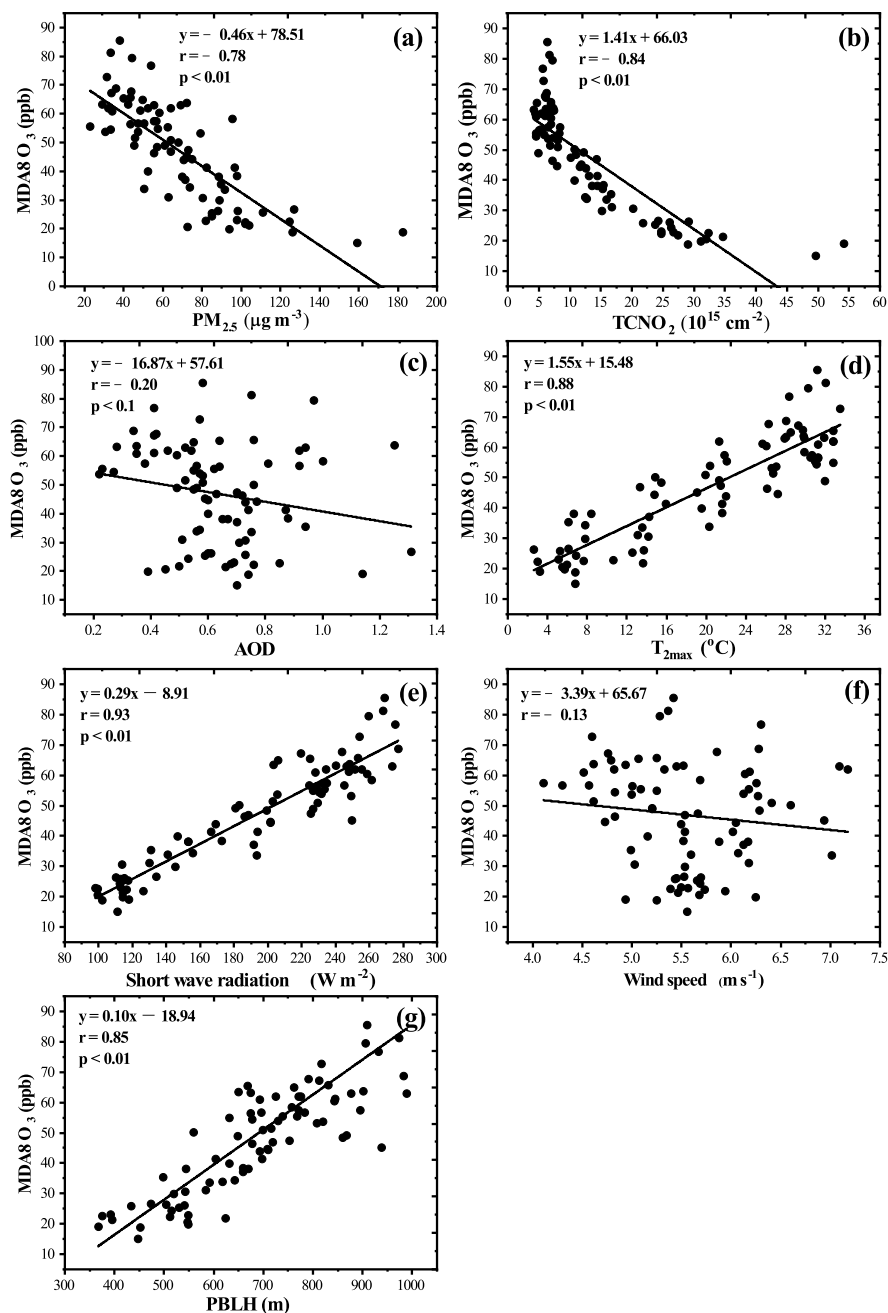
Figure 5. Response of MDA8 O$_3$ to (a) PM$_{2.5}$, (b) TCNO$_2$, (c) AOD, (d) T$_{2max}$, (e) shortwave radiation, (f) wind speed, and (g) PBLH observed in the NCP region, China during 2013–2019.

675
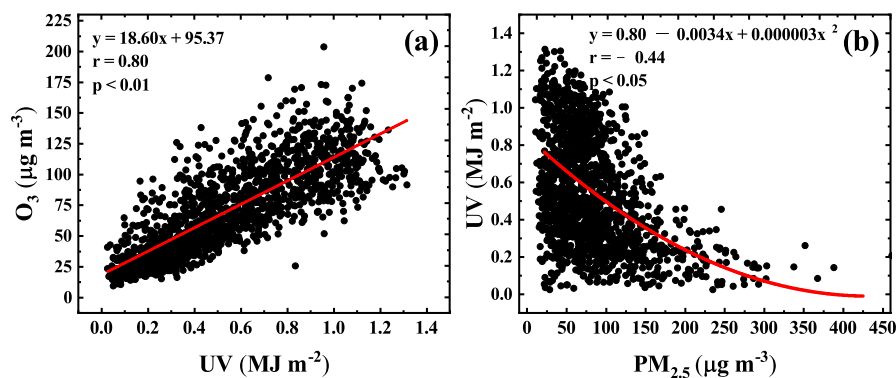
Figure 6. a) The relationships of surface O_3 concentrations (hourly) with (a) UV radiation and (b) UV radiation with

$PM_{2.5}$ concentrations based on the observations at Yucheng site during the time period of 08–17 LT in June, 2013–

2016.

680
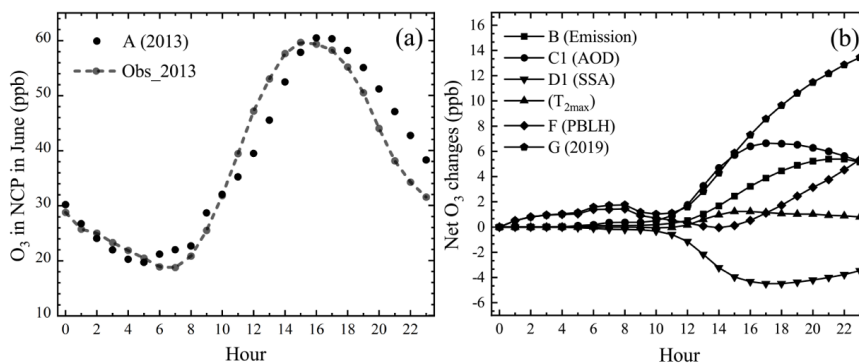
Figure 7. Comparisons of (a) regional averaged surface O_3 observations in NCP and simulated surface O_3 (A, control

685   case) and (b) simulated net changes in O_3 among different driving-factor conditions.

690
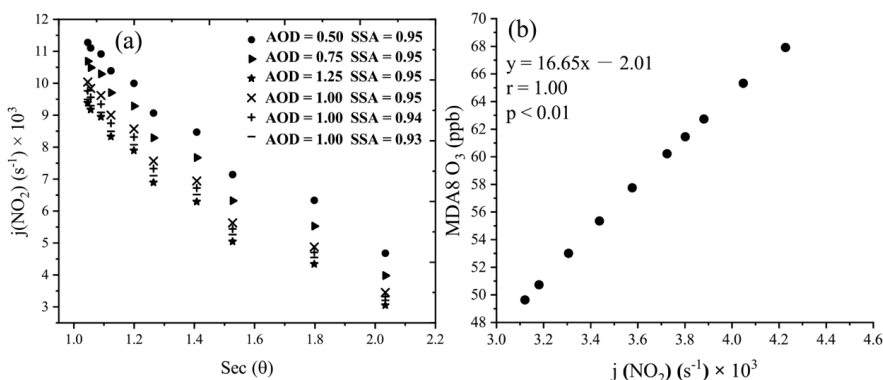
Figure 8. (a) response of photolysis rate of NO_2, $j(NO_2)$ to different values of aerosol optical depth (AOD) and single scatter factor (SSA) and (b) change in MDA8 O_3 with $j(NO_2)$ simulated by the MM model for the cases with SSA=0.95 and AOD varying from 0.5 to 1.25.
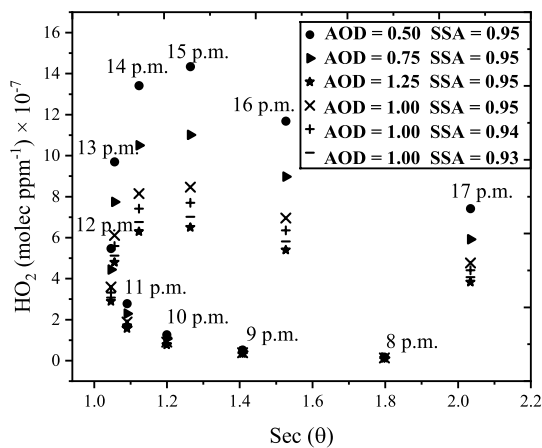
Figure 9. Response of concentrations of HO_2 to different values of aerosol optical depth (AOD) and single scatter factor (SSA).